Enhanced catalytic performance of molybdenum-doped mesoporous SBA-15 for metathesis of 1-butene and ethene to propene†

Chao Lin,[ab] Kai Tao,[a] Hongbo Yu,[a] Dayin Hua*[b] and Shenghu Zhou*[a]

Molybdenum-doped mesoporous SBA-15, mesoporous SBA-15-supported MoO_3/SBA-15, and traditional silica-supported MoO_3/SiO_2 were successfully synthesized. Various techniques, such as XRD, TEM, BET, UV-DRS, Raman, XPS and IR, were used to characterize the above obtained materials. The studies of TEM, XRD and BET confirmed that the highly ordered mesoporous structure of SBA-15 was maintained in the doped Mo-SBA-15 whereas supported MoO_3/SBA-15 showed a significant reduction in surface area due to the deposition of MoO_3 nanoparticles into the SBA-15 channels. XPS studies revealed that a high concentration of Mo^{5+} species appeared in doped Mo-SBA-15 whereas supported MoO_3/SBA-15 and MoO_3/SiO_2 only contained Mo^{6+} species. The metathesis reaction of 1-butene and ethene to propene was used to evaluate the catalytic performance of Mo-containing materials. The doped Mo-SBA-15 illustrated a superior catalytic performance over the supported MoO_3/SBA-15 and MoO_3/SiO_2 catalysts. The enhancement of catalytic performance for doped Mo-SBA-15 was assigned to the incorporation of Mo species into the SBA-15 framework. Due to the doping method, Mo-SBA-15 exhibited a well-ordered mesoporous structure, a high surface area, and a high concentration of Mo^{5+} species, which is beneficial to the catalytic performance for metathesis reactions.

1 Introduction

Metathesis reactions are currently used to synthesize complex organic molecules and polymers in an efficient and green way.[1–4] Due to the strong demand for propene on the worldwide market, the approach of using the metathesis of butene and ethene to yield propene has attracted increasing attention.[5] Supported tungsten,[6] molybdenum[7] and rhenium[8,9] oxides have been used as catalysts for propene formation through metathesis reactions. Among these catalysts, Re-containing catalysts are rarely used in industrial processes due to the high price of Re,[5] and supported tungsten and molybdenum oxides have received intense research because of their good catalytic stability and relatively low prices.[6,10,11]

The performance of supported molybdenum oxide catalysts for olefin metathesis is controlled by physicochemical properties of the supports, the oxidation states of the supported Mo species, and the pretreatment conditions.[12,13] A variety of materials have been chosen as supports for Mo-containing catalysts, such as Al_2O_3,[7] SiO_2–Al_2O_3,[14] MCM-48,[15] HMS[16] and HZSM-5.[17] The results have revealed a significant effect of the support on the catalytic performance of Mo-based catalysts. Huang *et al.*[10] prepared MoO_3/mordenite-alumina catalysts for the 1-butene metathesis reaction, and the catalysts treated with nitric acid have illustrated a much higher stability for propene formation. Liu *et al.*[18] reported that the Mo content as well as the hydrothermal treatment conditions have significant effects upon the catalytic performance of the Mo/Hβ-Al_2O_3 catalysts, and that the catalysts showed a superior catalytic performance over Mo/Al_2O_3, Mo/ZSM-35 and 6Mo/SAPO-11 for the metathesis of ethene and 2-butene to propylene.

Due to their high surface areas, well-ordered structures and narrow pore size distributions, application of mesoporous materials in olefin metathesis catalysts is promising.[19] Balcar *et al.*[9] studied the catalytic performances of various mesoporous Al_2O_3-supported Re-based catalysts and found that all catalysts investigated exhibited more than one order of magnitude higher activity than a commercial catalyst with a large pore distribution and a considerable microporous fraction under the same reaction conditions. Bhuiyan *et al.*[20] synthesized W-containing mesoporous SBA-15 and MCM-41 by a direct hydrothermal method for the metathesis of 2-butene to propene, and the catalytic results

[a] *Ningbo Institute of Materials Technology and Engineering, Chinese Academy of Sciences, Ningbo, Zhejiang 315201, PR China. E-mail: zhoush@nimte.ac.cn*
[b] *Department of Physics, Faculty of Science, Ningbo University, Ningbo, Zhejiang 315211, PR China. E-mail: huadayin@nbu.edu.cn; Fax: +86574 86685043; Tel: +86574 86696927*

revealed that the catalytic activity of the W-MCM-41 catalysts was higher than that of W-SBA-15. The well-dispersed active tetrahedral tungsten oxide species were attributed to being the origin of the catalytic performance enhancement. Balcar *et al.*[21] prepared Mo-containing catalysts for the metathesis of 1-dodecene and 1-tetradecene by supporting molybdenum dioxide bis(acetylacetonate) and molybdenum dioxide bis(glycolate) on SBA-15, and found that the SBA-15-supported catalysts exhibited a higher activity than the MCM-41-supported catalysts. In addition, Mo-containing mesoporous materials have also shown an excellent performance for many other reactions, such as with MoO_3/SBA-15 for the selective oxidation of methane,[22] Mo-SBA-15 for the selective oxidation of propene[23] and the epoxidation of olefins.[24]

We have previously reported the tungsten-doped mesoporous KIT-6 (W-KIT-6) catalyst for the metathesis of 1-butene and ethene to propene, and found that the doped W-KIT-6 illustrated a superior catalytic performance over supported WO_3/KIT-6 and WO_3/SiO_2 catalysts.[25] Here, we report the first successful application of doped Mo-SBA-15 catalysts for the production of propene from the metathesis reaction of 1-butene and ethene, and we compare the catalytic performance of doped Mo-SBA-15 with supported MoO_3/SBA-15 and MoO_3/SiO_2 catalysts. The schematic demonstration of this study is shown in Scheme 1. Doped Mo-SBA-15 was synthesized by a modified one-pot method,[24] and the supported MoO_3/SBA-15 and MoO_3/SiO_2 catalysts were synthesized by a traditional impregnation method using SBA-15 or traditional SiO_2 as the supports. The superior catalytic performance of Mo-SBA-15 catalysts for the metathesis of 1-butene and ethene to propene demonstrates a good example of the enhancement of catalytic performance due to the highly dispersed active species through doping methods.

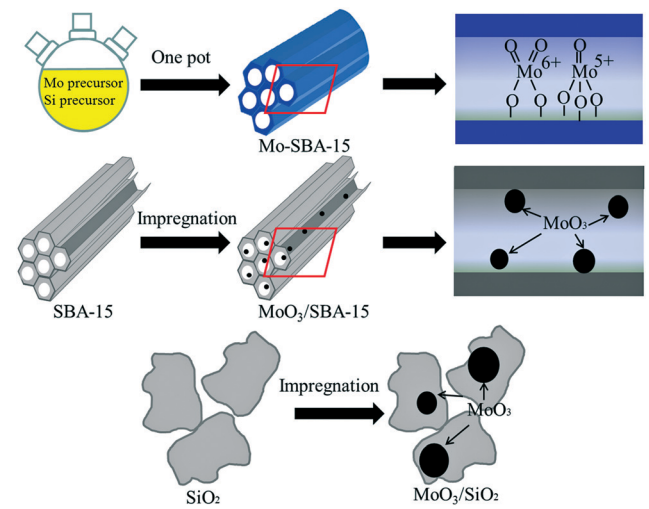

Scheme 1 Schematic diagram showing the synthesis of doped mesoporous Mo-SBA-15, supported mesoporous MoO_3/SBA-15 and traditional MoO_3/SiO_2.

2 Experimental

2.1 Chemicals

Poly(ethylene glycol)-block-poly(propylene glycol)-block-poly(ethylene glycol) (P123, M = 5800) was purchased from Sigma-Aldrich. Tetraethyl orthosilicate (TEOS, AR grade) was purchased from Aladdin. Ammonium paramolybdate ($(NH_4)_6Mo_7O_{24}{\cdot}4H_2O$) and hydrochloric acid (HCl, AR grade) were purchased from Shanghai Chemical Reagent Company. Silica gel (surface area, 399 $m^2\ g^{-1}$) was obtained from Qingdao Haiyang Chemical Co. Ltd. All the reagents were used as received.

2.2 Catalyst preparation

2.2.1 Preparation of SBA-15. The SBA-15 was synthesized using a modified reported method.[26,27] Briefly, 4 g of P123, 6.1 g of 35 wt% HCl and 125 g deionized water were mixed in a 250 mL three-necked flask. After vigorous stirring at 40 °C for 1 hour, 8.5 g of TEOS were added dropwise into the solution followed by stirring for another 24 h. The above mixture was then transferred to a Teflon-lined autoclave, and was heated at 100 °C for another 24 h. Finally, the powdery solid products were obtained by filtration, washing with deionized water, and calcining in a muffle oven at 550 °C for 4 h with a ramping rate of 1 °C min^{-1} to remove the P123 surfactants.

2.2.2 Preparation of doped Mo-SBA-15. The doped Mo-SBA-15 was synthesized according to the procedures reported by Melero *et al.*[24] In a typical synthesis of Mo-SBA-15, 3 g of P123 was dissolved in an aqueous solution containing 100 g of deionized water and 6.1 g of 35 wt% HCl. The resulting solution was vigorously stirred at 40 °C for 1 h. Appropriate amount of ammonium paramolybdate dissolved in 25 g of deionized water was added into the above mixture. The resultant yellow solution was stirred for at least 3 h to guarantee the complexation of Mo(VI) species with the poly(ethylene oxide) chains and give a clear solution. Then, 8.5 g of TEOS was added dropwise into the above solution. The obtained mixture was vigorously stirred at 40 °C for 24 h, and was then transferred to a Teflon-lined autoclave followed with heating at 100 °C for another 24 h. After cooling to room temperature, the light blue powdery products were collected, washed, and calcined using the same procedure as for SBA-15. Five catalysts with Mo contents of 1.3, 2.2, 3.0, 5.1, and 10.8% (determined by inductively coupled plasma-optical emission spectroscopy (ICP-OES)) were prepared, and are denoted as Mo-SBA-15-1.3%, Mo-SBA-15-2.2%, Mo-SBA-15-3.0% Mo-SBA-15-5.1%, and Mo-SBA-15-10.8%, respectively.

2.2.3 Preparation of supported MoO_3/SBA-15 and MoO_3/SiO_2. The supported MoO_3/SBA-15 catalysts were prepared using an impregnation method. Typically, an appropriate amount of ammonium paramolybdate was dissolved in 3 g of H_2O. To this clear solution, 1.5 g calcined SBA-15 was added. The mixture was ultrasonicated for 20 min. Then, the H_2O was evaporated at 100 °C for 24 h in a drying oven.

The dried powders were calcined using the same procedure as for SBA-15. The supported MoO_3/SiO_2 catalysts were prepared by impregnating 1.5 g of the support powders with an aqueous solution containing the required amount of ammonium paramolybdate and 10 g of deionized water followed by sonication and stirring for 20 min. After drying in an oven at 100 °C overnight, the powders were calcined using the same procedure as for SBA-15. These two catalysts were denoted as MoO_3/SBA-15-3.0% and MoO_3/SiO_2-3.0% according to the real Mo loading by ICP-OES.

2.3 Catalyst characterization.

Inductively coupled plasma-optical emission spectroscopy (ICP-OES) analysis was achieved to obtain the real Mo loading using a Perkin-Elmer OPTIMA 2100 DV optical emission spectrometer. Transmission electron microscopy (TEM) images were obtained using a JEOL 2100 transmission electron microscope operated at 200 kV. X-ray photoelectron spectroscopy (XPS) studies of the Mo-containing catalysts were obtained using an AXIS ULTRA DLD multifunctional X-ray photoelectron spectrometer with an Al source. CaseXPS software was used to perform the data processing. The X-ray diffraction (XRD) samples were analyzed using a Bruker D8 Avance X-ray diffractometer using Cu Kα radiation in the 2θ range of 0.5–5 and 10–90°. UV-vis diffuse reflectance spectra (UV-DRS) between 200 and 800 nm were obtained using PE lambda 950 equipment using $BaSO_4$ as a reference. The infrared (IR) spectra were achieved using a Bruker Tensor 27 spectrophotometer. The Raman spectra were obtained using a Renishaw Raman Spectrometer equipped with a microscope (laser wavelength, 532 nm).

The Brunauer–Emmett–Teller (BET) surface area, pore size distribution, pore volume, and adsorption–desorption isotherm of the samples were measured by N_2 physical adsorption at 77 K using a Micromeritics ASAP-2020 M adsorption apparatus. The specific surface area was determined by the Brunauer–Emmett–Teller (BET) method. The pore size distribution was obtained using multiple Barrett–Joyner–Halenda (BJH) methods, using the adsorption branches of the nitrogen adsorption–desorption isotherm. All samples were degassed under vacuum at 200 °C for 5 h before testing. Post-reaction catalysts were measured using a Pyris Diamond thermogravimetric analyzer (TGA) to identify the carbon deposition. The samples were heated from 30 to 800 °C at a heating rate of 10 °C min^{-1} at an air atmosphere with a gas flow rate of 50 mL min^{-1}.

2.4 Catalyst test

The metathesis reaction of 1-butene and ethene to propene was performed in a fixed-bed reactor (i.d. 10 mm). In a typical test, 1 g of Mo-containing catalyst with a 20–40 mesh size were placed in the center of the reactor, and above and below were layers of inert SiO_2 beads. Before the catalytic tests, the catalyst was activated at 550 °C for 4 h to remove the moisture in a pure N_2 stream at a flow rate of 35 mL min^{-1} at 0.1 MPa. After the reactor had cooled down to the catalytic reaction temperature, ethene and 1-butene were then fed into the system. The metathesis reaction was carried out at 350–500 °C, 0.1 MPa, a weight hourly space velocity (WHSV) of 2.0 h^{-1} (1-C_4H_8 + C_2H_4) and a molar ratio of 1/2 of 1-butene/ethene. The start of the reaction time was set to the time point after one hour of reactant gas feeding, and the products were detected online using a gas chromatograph (GC) with a flame ionization detector (FID). The 1-butene conversion and propene selectivity were calculated according to the literature,[23]

$$C_{1\text{-butene}} = \frac{[C_3]_n/2 + [2-C_4]_n}{[C_3]_n/2 + [1-C_4]_n + [2-C_4]_n}$$

$$S_{\text{propene}} = \frac{[C_3]_n/2}{[C_3]_n/2 + [2-C_4]_n}$$

$$S_{2\text{-butene}} = \frac{[2-C_4]_n}{[C_3]_n/2 + [2-C_4]_n}$$

where $C_{1\text{-butene}}$, S_{propene}, $S_{2\text{-butene}}$ are the 1-butene conversion, propene selectivity, and 2-butene selectivity, and where $[C_3]_n$, $[1-C_4]_n$ and $[2-C_4]_n$ are the molar percentage of propene, 1-butene, and 2-butene in the effluent gases, respectively.

3 Results and discussion

The doped Mo-SBA-15 catalysts were synthesized using a modified reported method.[24] Ammonium paramolybdate and TEOS were used as the Mo precursor and Si precursor in the synthesis of Mo-SBA-15. Mesoporous SBA-15-supported MoO_3/SBA-15 and traditional silica-supported MoO_3/SiO_2 catalysts were synthesized using a wet impregnation method. The real Mo loadings in all of the Mo-containing catalysts were determined by ICP-OES.

The structures of the Mo-containing materials were measured by TEM. Fig. 1 shows the TEM images of Mo-SBA-15, MoO_3/SBA-15 and MoO_3/SiO_2. As shown in Fig. 1a, a highly ordered mesoporous structure was observed in SBA-15, which is consistent with the literature.[27,28] The well-ordered mesoporous structures were also observed in Mo-SBA-15-1.3% in Fig. 1b, Mo-SBA-15-2.2% in Fig. 1c, Mo-SBA-15-3.0% in Fig. 1d, and Mo-SBA-15-5.1% in Fig. 1e. However, the well-ordered mesoporous structure disappeared in Mo-SBA-15-10.8% in Fig. 1f, suggesting the collapse of the structure by introduction of too many Mo species. For all Mo-SBA-15 materials, the MoO_3 particles were not observed even at a high Mo loading of 10.8 wt%, suggesting a high dispersion of Mo species by the doping method. In contrast, MoO_3 particles were observed in the supported Mo-containing materials. As shown in Fig. 1g for the MoO_3/SBA-15 catalyst, nanosized MoO_3 particles were confined in the channels of SBA-15 with some particles present on the outer surfaces. The mean size

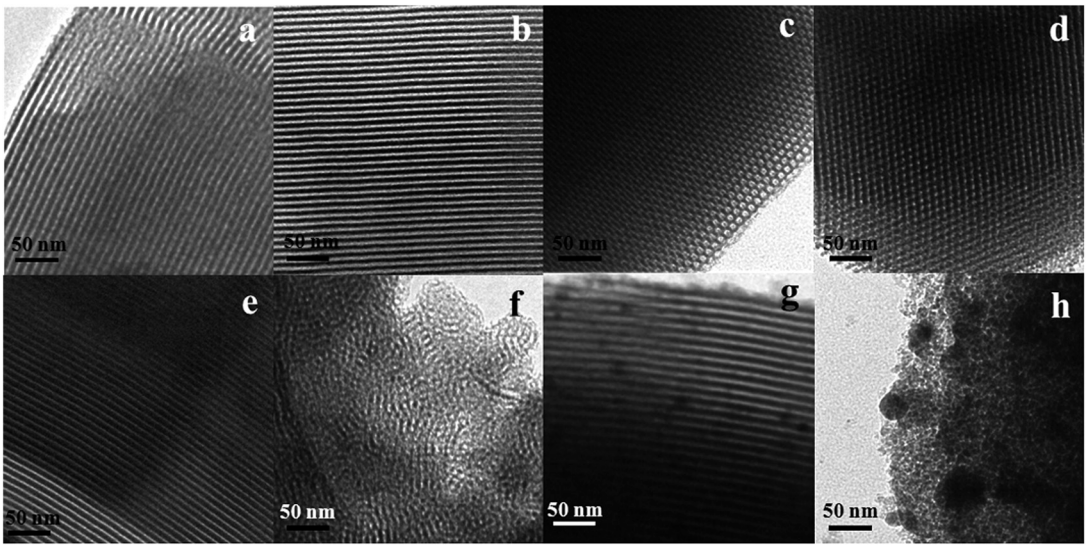

Fig. 1 TEM images showing (a) SBA-15; (b) Mo-SBA-15-1.3%; (c) Mo-SBA-15-2.2%; (d) Mo-SBA-15-3.0%; (e) Mo-SBA-15-5.1%; (f) Mo-SBA-15-10.8%; (g) MoO_3/SBA-15-3.0%; and (h) MoO_3/SiO_2-3.0%.

of MoO_3 particles is around 5.9 nm, acquired by counting 100 randomly chosen particles, as shown in the ESI† (Fig. S1). However, bulk MoO_3 aggregations were present in Fig. 1h when using traditional SiO_2 as the support.

To analyze the oxidation states of Mo species in Mo-containing catalysts, XPS studies were carried out. Fig. 2 summarized XPS spectra of Mo-SBA-15, MoO_3/SBA-15 and MoO_3/SiO_2. The theory of Doniach and Sunjic is exploited to fit XPS curves.[29] As shown in Fig. 2a, Mo-SBA-15-2.2% contained two Mo species. The binding energies of 232.5 eV/235.6 eV and 231.1 eV/234.2 eV were assigned to the binding energies of $3d_{5/2}/3d_{3/2}$ of Mo^{6+} and Mo^{5+} species,[30] respectively. The appearance of Mo^{6+} and Mo^{5+} species was also observed for Mo-SBA-15-3.0% in Fig. 2b and Mo-SBA-15-5.1% in Fig. 2c. However, only Mo^{6+} species was observed for Mo-SBA-15-10.8% in Fig. 2d when the Mo loading increased to 10.8%. The XPS spectra of MoO_3/SBA-15-3.0% in Fig. 2e and MoO_3/SiO_2-3.0% in Fig. 2f only exhibited the binding energies of Mo^{6+} species, which is consistent with literature.[31,32] Various oxidation states of Mo species have been reported in Mo-containing materials depending on preparation methods or treatment conditions.[30,33] The different oxidation states of Mo species may influence their catalytic metathesis of 1-butene and ethene to propene.

The molar percentage of Mo species with different oxidation states in Mo-containing catalysts are illustrated in Table 1. For quantitative analysis, a single spin–orbit splitting of 3.1 eV and a single spin–orbit doublet with a fixed area ratio of 3/2 were used, as well as the full width at half maximum (FWHM) which was limited to under 2.4 eV.[34] The molar percentages of Mo^{6+} species in traditional silica-supported MoO_3/SiO_2-3.0% and mesoporous SBA-15-supported MoO_3/SBA-15-3.0% are 100%, indicating only the presence of fully oxidized Mo species. In contrast, Mo-SBA-15-2.2%, Mo-SBA-15-3.0% and Mo-SBA-15-5.1% contained 44.0–67.5% of Mo^{5+} species, indicating the incorporation of Mo species into the SBA-15 framework. The previously reported W-SBA-15 catalyst contained five incorporation models of W species into the SBA-15 framework, and W^{5+} species were present within three of the models.[35] In the present study, a high concentration of Mo^{5+} species in Mo-SBA-15 with a certain range of Mo loading is possibly induced in a similar way. These Mo^{5+} species in Mo-SBA-15 may be beneficial to the catalytic performance for the metathesis of 1-butene and ethene to propene.[36] When the Mo loading increased to 10.8 wt%, 100% of Mo^{6+} species was observed in Mo-SBA-15-10.8%, suggesting that the Mo species were no longer doped into the framework due to the structure collapse confirmed by Fig. 1f.

The small-angle XRD patterns of SBA-15 and Mo-SBA-15 with different Mo loadings are shown in Fig. 3. SBA-15 in Fig. 3a exhibited (100), (110) and (200) diffractions, which is consistent with the literature.[26,27] No significant change was observed between SBA-15 in Fig. 3a and Mo-SBA-15-1.3% in Fig. 3b, indicating the maintenance of long-range order at the low Mo loading of 1.3 wt%. As the molybdenum loading increased from 1.3 to 5.1 wt%, the diffraction intensities became weaker, indicating the decrease of long-range order due to the incorporation of more Mo species into the SBA-15 framework. When the Mo loading was increased to 10.8 wt%, Mo-SBA-15-10.8% in Fig. 3f illustrates very weak (100) diffraction without (110) and (200) diffractions, suggesting the collapse of long-range order due to the incorporation of too many Mo species into framework, which is consistent with the TEM observation in Fig. 1f.

The N_2 adsorption–desorption isotherms of SBA-15, MoO_3/SBA-15, Mo-SBA-15 are shown in Fig. 4, and their corresponding textural properties are listed in Table 2. The isotherms of SBA-15 in Fig. 4a, Mo-SBA-15-1.3% in Fig. 4b, Mo-SBA-15-2.2% in Fig. 4c, Mo-SBA-15-3.0% in Fig. 4d, Mo-SBA-15-5.1%

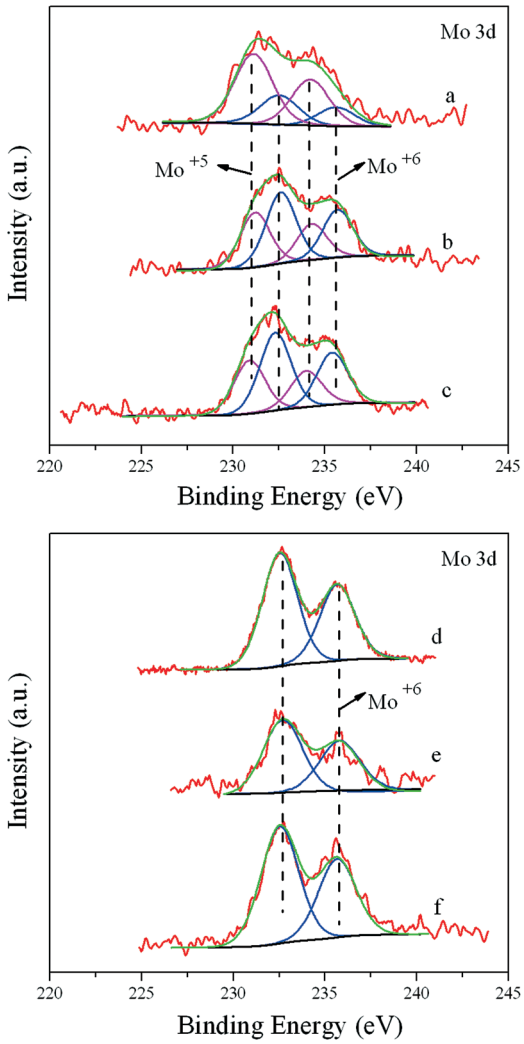

Fig. 2 XPS spectra showing (a) Mo-SBA-15-2.2%; (b) Mo-SBA-15-3.0%; (c) Mo-SBA-15-5.1%; (d) Mo-SBA-15-10.8%; (e) MoO_3/SBA-15-3.0%; and (f) MoO_3/SiO_2-3.0%.

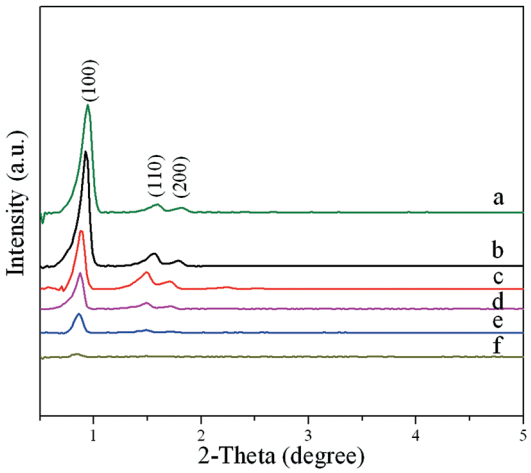

Fig. 3 Small-angle XRD patterns of various samples showing (a) SBA-15; (b) Mo-SBA-15-1.3%; (c) Mo-SBA-15-2.2%; (d) Mo-SBA-15-3.0%; (e) Mo-SBA-15-5.1%; and (f) Mo-SBA-15-10.8%.

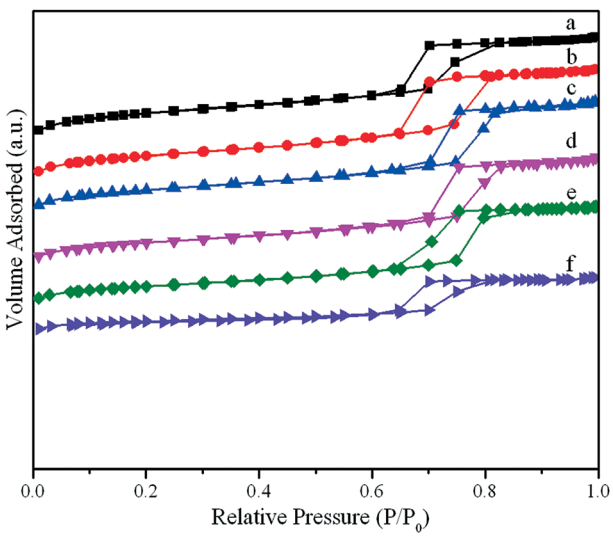

Fig. 4 N_2 adsorption–desorption isotherms showing (a) SBA-15; (b) Mo-SBA-15-1.3%; (c) Mo-SBA-15-2.2%; (d) Mo-SBA-15-3.0%; (e) Mo-SBA-15-5.1%; and (f) MoO_3/SBA-15-3.0%.

in Fig. 4e, and MoO_3/SBA-15-3.0% in Fig. 4f showed typical type IV isotherms with the H1-type hysteresis loop, obviously indicating that those materials possessed a mesoporous structure.[21,27] As presented in Table 2, the BET surface area of SBA-15 was 923 $m^2\ g^{-1}$. When Mo species was incorporated into the SBA-15 framework, the surface area of Mo-SBA-15-1.3% was 811 $m^2\ g^{-1}$, showing a slight decrease of surface area. The surface area of Mo-SBA-15 decreased with the Mo loading increasing, and reached 440 $m^2\ g^{-1}$ for Mo-SBA-15-10.8% due to the collapse of well-ordered mesoporous structure at a high Mo loading. The surface area of doped Mo-SBA-15-3.0% was 714 $m^2\ g^{-1}$. In contrast, the supported

Table 1 Distribution of oxidation states of molybdenum in Mo-containing materials by XPS

Catalyst	Binding energies of Mo_{3d} (eV)				Mo^{5+} (%)	Mo^{6+} (%)
	$Mo^{6+}3d_{5/2}$	$Mo^{6+}3d_{3/2}$	$Mo^{5+}3d_{5/2}$	$Mo^{5+}3d_{3/2}$		
Mo-SBA-15-2.2%	232.5	235.6	231.1	234.2	67.5	32.5
Mo-SBA-15-3.0%	232.6	235.7	231.2	234.3	44.0	56.0
Mo-SBA-15-5.1%	232.5	235.6	231.2	234.3	46.4	53.6
Mo-SBA-15-10.8%	232.4	235.5	N/A	N/A	0	100
MoO_3/SBA-15-3.0%	232.6	235.7	N/A	N/A	0	100
MoO_3/SiO_2-3.0%	232.5	235.6	N/A	N/A	0	100

Table 2 BET surface areas, pore volumes, and pore sizes of SBA-15 and Mo-containing materials

Catalyst	BET surface area ($m^2\ g^{-1}$)	Pore volume ($cm^3\ g^{-1}$)	Pore size (nm)
SBA-15	923	1.17	5.0
Mo-SBA-15-1.3%	811	1.22	6.0
Mo-SBA-15-2.2%	787	1.24	6.3
Mo-SBA-15-3.0%	714	1.17	6.5
Mo-SBA-15-5.1%	634	1.08	6.8
Mo-SBA-15-10.8%	440	0.87	7.9
MoO_3/SBA-15-3.0%	466	0.61	6.9
MoO_3/SiO_2-3.0%	350	0.85	9.7

MoO_3/SBA-15-3.0% was 466 $m^2\ g^{-1}$, showing a significant decrease compared to Mo-SBA-15 at the same Mo loading. The significant reduction of surface areas of MoO_3/SBA-15 indicated that parts of pores of SBA-15 were blocked due to the impregnation method. By comparison of surface areas of doped and supported materials at the same Mo loading, the surface areas decreased as the following sequence: Mo-SBA-15 > MoO_3/SBA-15 > MoO_3/SiO_2.

The Raman spectra of SBA-15, Mo-SBA-15, MoO_3/SBA-15 and MoO_3/SiO_2 are illustrated in Fig. 5. SBA-15 in Fig. 5a shows a band around 497 cm^{-1}, which is attributed to cyclic tetrasiloxane rings.[37] The bands around 607 and 977 cm^{-1} could be assigned to cyclic trisiloxane rings and the Si–OH stretching mode,[37] respectively. Fig. 5g illustrates the Raman spectrum of traditional MoO_3/SiO_2-3.0%. The bands at 818 and 991 cm^{-1} are attributed to crystalline α-MoO_3,[24,37] which is consistent with the large MoO_3 particles shown by the TEM study in Fig. 1h. However, for the Mo-SBA-15 materials with a Mo loading from 1.3 to 5.1 wt% in Fig. 5b–e, the band around 973–976 cm^{-1} becomes weak, and the band around 818 cm^{-1} is almost invisible, suggesting the presence of highly dispersed Mo species within the doped Mo-SBA-15. Supported MoO_3/SBA-15-3.0% in Fig. 5f shows a similar Raman spectrum to that of Mo-SBA-15, which is consistent with the small MoO_3 nanoparticles in the mesoporous channels of SBA-15 shown by the TEM study in Fig. 1g.

The diffuse reflectance spectra in the UV region of various samples are shown in Fig. 6. All the Mo-containing samples exhibited three bands, around 220, 256 and 320 nm. The bands around 220 and 256 nm can be attributed to the tetrahedral molybdate species, which indicates a good dispersion of Mo species.[38] The broad band around 320 nm was assigned to the Mo–O–Mo bridge bond of octahedral species,[10] which indicates relatively large Mo species.[38] For Mo-SBA-15 in Fig. 6b–e and MoO_3/SBA-15 in Fig. 6f, the dominant bands are at 220 and 256 nm, suggesting a high dispersion of Mo species in the doped Mo-SBA-15 and supported MoO_3/SBA-15 materials. However, the spectrum of traditional silica-supported MoO_3/SiO_2-3.0% in Fig. 6g illustrates an intense band around 320 nm, suggesting the high concentration of octahedral molybdate. The presence of dominant octahedral molybdate in MoO_3/SiO_2-3.0% is consistent with the finding of large MoO_3 particles in TEM image of MoO_3/SiO_2, as shown in Fig. 1h.

The wide-angle XRD patterns of various Mo-containing samples are shown in Fig. 7. A typical peak of amorphous silica in the 2θ range from 15 to 35° is observed for all of the Mo-containing materials. The XRD profiles of Mo-SBA-15-

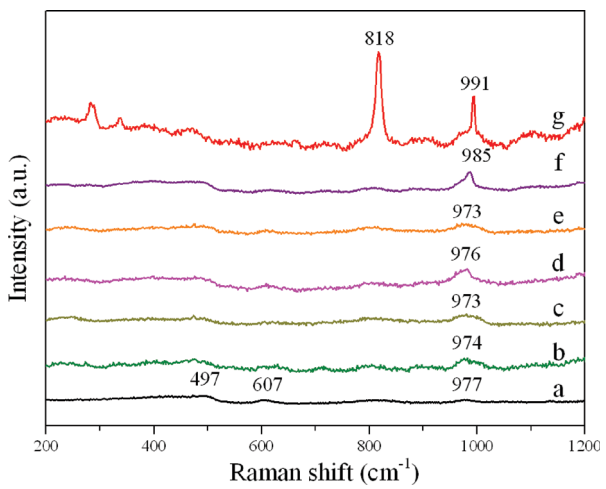

Fig. 5 Raman spectra showing (a) SBA-15; (b) Mo-SBA-15-1.3%; (c) Mo-SBA-15-2.2%; (d) Mo-SBA-15-3.0%, (e) Mo-SBA-15-5.1%; (f) MoO_3/SBA-15-3.0%; and (g) MoO_3/SiO_2-3.0%.

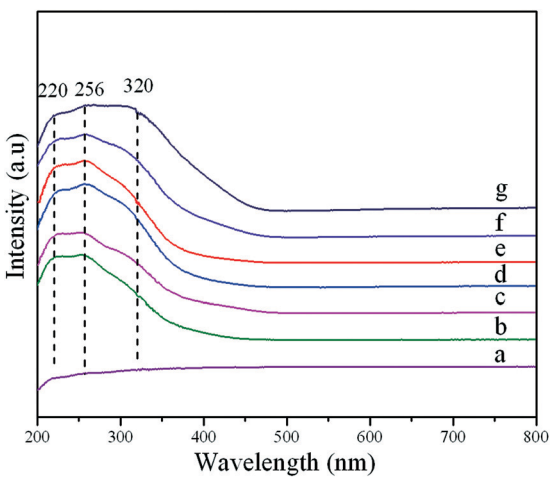

Fig. 6 Diffuse reflectance UV-vis spectra showing (a) SBA-15; (b) Mo-SBA-15-1.3%; (c) Mo-SBA-15-2.2%; (d) Mo-SBA-15-3.0%; (e) Mo-SBA-15-5.1%; (f) MoO_3/SBA-15-3.0%; and (g) MoO_3/SiO_2-3.0%.

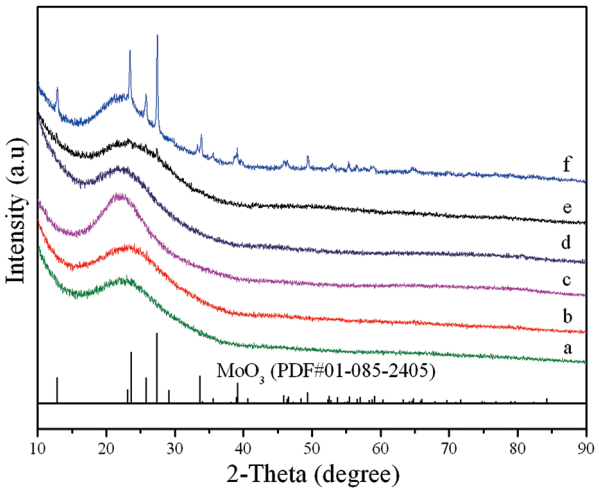

Fig. 7 Wide-angle XRD profiles of different Mo-containing materials showing (a) Mo-SBA-15-3.0%; (b) MoO_3/SBA-15-3.0%; (c) MoO_3/SiO_2-3.0%; (d) Mo-SBA-15-10.8%; (e) MoO_3/SBA-15-10.8%; and (f) MoO_3/SiO_2-10.8%.

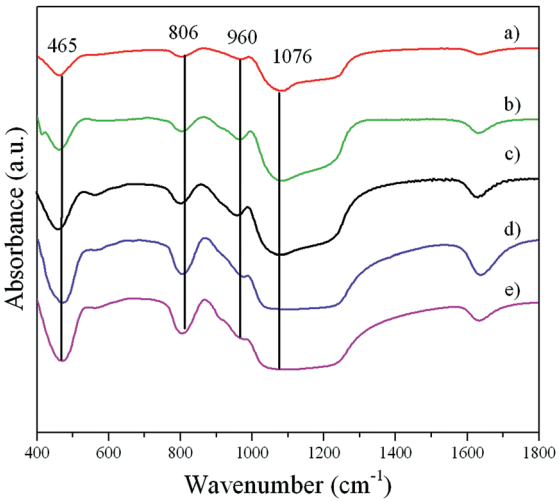

Fig. 8 FTIR spectra of various samples showing (a) SBA-15; (b) Mo-SBA-15-2.2%; (c) Mo-SBA-15-5.1%; (d) MoO_3/SBA-15-3.0%; and (e) MoO_3/SiO_2-3.0%.

3.0%, MoO_3/SBA-15-3.0% and MoO_3/SiO_2-3.0% are shown in Fig. 7a–c, respectively. At this low Mo loading of 3.0 wt%, no MoO_3 diffractions are observed although the TEM image of MoO_3/SiO_2-3.0% in Fig. 1h suggested the presence of large MoO_3 particles. Fig. 7d–f shows the XRD profiles of Mo-SBA-15-10.8%, MoO_3/SBA-15-10.8% and MoO_3/SiO_2-10.8%, respectively. At this high Mo loading of 10.8 wt%, no MoO_3 diffractions are observed for Mo-SBA-15-10.8% whereas slight MoO_3 diffractions are observed for supported MoO_3/SBA-15-10.8%. In contrast, the XRD profile of supported MoO_3/SiO_2-10.8% exhibits intense MoO_3 diffractions. These XRD studies reveal that the dispersion of Mo species decreases in the following sequence: doped Mo-SBA-15 > supported MoO_3/SBA-15 > supported MoO_3/SiO_2, which is consistent with the TEM images in Fig. 1.

The FTIR spectra of SBA-15 and the Mo-containing samples are shown in Fig. 8. The characteristic absorption bands at 465, 806 and 1076 cm^{-1} are attributed to the rocking vibration, symmetric stretching vibration and antisymmetric stretching vibration of [SiO_4], respectively. The band at 960 cm^{-1} could be assigned to a stretching vibration of a [SiO_4] unit bonded to heteroatoms or the absorption peak of Si–OH groups.[39–41]

The metathesis reaction of 1-butene and ethene to propene was used to evaluate the catalytic performance of our Mo-containing catalysts.[7,20] The above reaction proceeds through the well-known carbine-metallacycle mechanism,[7] and possible reaction pathways are shown in eqn (1)–(6). For the metathesis of 1-butene and ethene to propene, 1-butene has to isomerize to 2-butene for propene formation. Propene may come from reaction of 1-butene and 2-butene (eqn (3)) or reaction of ethene and 2-butene (eqn (4)). An increase in the ethene/1-butene ratio will favor propene formation and decrease the selectivity of olefins with a high molecular weight in eqn (6). In this study, the metathesis reaction over Mo-containing catalysts was carried out in a micro-reactor at a temperature range from 350 to 500 °C, and a ratio of 1-butene/ethene of 1/2 was used to obtain a high propene selectivity.

$$2CH_3CH_2CH{=}CH_2 \rightleftharpoons CH_2{=}CH_2 + CH_3CH_2CH{=}CHCH_2CH_3 \quad (1)$$

$$CH_3CH_2CH{=}CH_2 \rightleftharpoons CH_3CH{=}CHCH_3 \quad (2)$$

$$CH_3CH_2CH{=}CH_2 + CH_3CH{=}CHCH_3 \rightleftharpoons CH_3CH{=}CH_2 + CH_3CH_2CH{=}CHCH_3 \quad (3)$$

$$CH_3CH{=}CHCH_3 + CH_2{=}CH_2 \rightleftharpoons 2CH_3CH{=}CH_2 \quad (4)$$

$$CH_3CH_2CH{=}CH_2 + CH_3CH{=}CH_2 \rightleftharpoons CH_2{=}CH_2 + CH_3CH_2CH{=}CHCH_3 \quad (5)$$

$$nCH_3CH_2CH{=}CH_2 \rightleftharpoons (C_4H_8)_n \quad (6)$$

The careful analysis of products suggested that the main products of the metathesis of 1-butene/ethene over all of the Mo-SBA-15, MoO_3/SBA-15 and MoO_3/SiO_2 catalysts were 2-butene and propene. Only a trace amount (less than 0.1%) of byproducts was found. Therefore, the conversion of 1-butene ($C_{1\text{-butene}}$), the selectivity of propene (S_{propene}), and the selectivity of 2-butene ($S_{2\text{-butene}}$) were used to evaluate the performances of the different catalysts. The conversion of 1-butene and selectivity of propene and 2-butene for the 3.0 wt% Mo-containing catalysts at the reaction temperature of 450 °C are presented in Fig. 9. The average conversion of 1-butene, and selectivities of propene and 2-butene over traditional MO_3/SiO_2-3.0% were 50.0, 74.0 and 26.0%, respectively. For supported MoO_3/SBA-15-3.0%, the 1-butene conversion, propene and 2-butene selectivities were 55.8, 77.2 and 22.8%, showing a better catalytic performance than that of

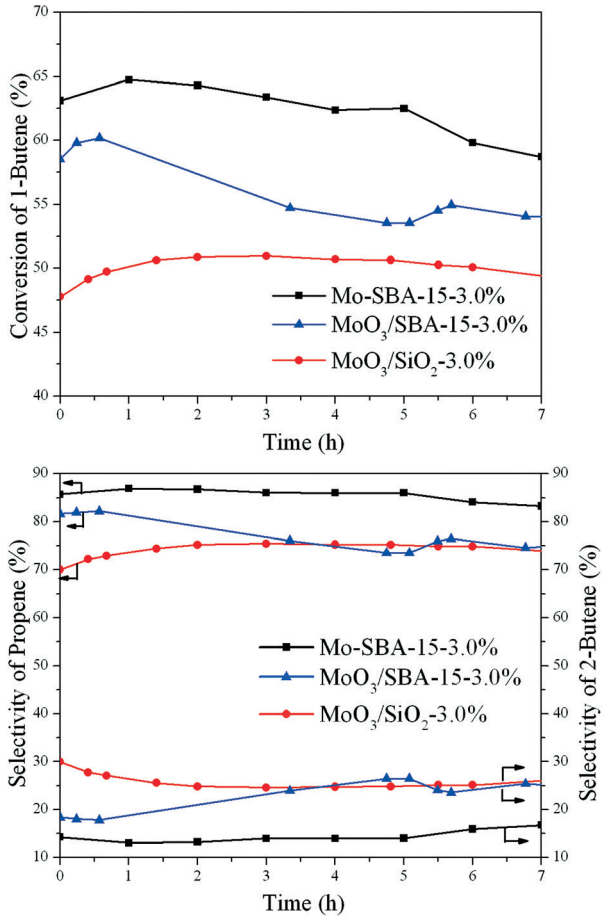

Fig. 9 1-Butene conversion (upper panel), and selectivities of propene and 2-butene (lower panel) over 3.0 wt% Mo-containing catalysts. Reaction conditions: T = 450 °C; P = 0.1 MPa; 1-C_4H_8/C_2H_4 = 1/2; WHSV (1-C_4H_8 + C_2H) of 2.0 h^{-1}; Mo-containing catalyst = 1.0 g.

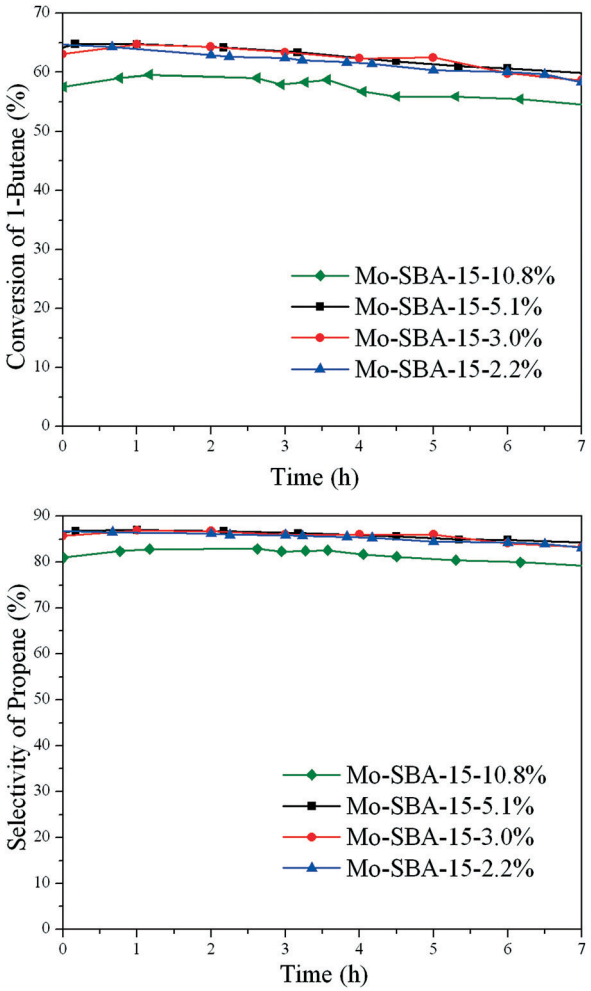

Fig. 10 1-Butene conversion (upper panel) and propene selectivity (lower panel) over Mo-SBA-15 catalysts with different Mo loadings. Reaction conditions: T = 450 °C; P = 0.1 MPa; 1-C_4H_8/C_2H_4 = 1/2; WHSV (1-C_4H_8 + C_2H_4) of 2.0 h^{-1}; Mo-containing catalyst = 1.0 g.

the traditional silica-supported MO_3/SiO_2-3.0%. The average 1-butene conversion and propene selectivity over doped Mo-SBA-15-3.0% were 62.4 and 85.6%, respectively, and the 2-butene selectivity was only 14.4%, illustrating the best catalytic performance.

Since the BET surface area of Mo-SBA-15-3.0% is about twice of that of MO_3/SiO_2-3.0%, the catalytic performance of 2 g of the Mo/SiO_2-1.5% catalyst was carried out to keep the same amount of Mo and the same total BET surface as Mo-SBA-15-3.0% (1 g) under the same reaction conditions. The Mo/SiO_2-1.5% with double-weighting showed around 45% 1-butene conversion and 64% propene selectivity, as shown in Fig. S2.† Compared with the performance of the double amount of Mo/SiO_2-1.5% catalyst, the Mo-SBA-15-3.0% still exhibited an improved catalytic performance, even though the amount of Mo and total BET surface area are the same for both catalysts, proving the efficiency of the doping method for the preparation of a highly active metathesis catalyst. Here, it should be mentioned that literature has reported highly active MoO_3/SBA-15 for the metathesis of higher 1-alkenes by adopting organic Mo complexes as precursors,[19,21] suggesting the importance of the Mo precursors in addition to the doping method in this study.

The catalytic performances of Mo-SBA-15 with different Mo loadings are illustrated in Fig. 10. The average 1-butene conversion and propene selectivity over Mo-SBA-15-2.2% were 61.7 and 85.3%, respectively. With increased Mo loading, Mo-SBA-15-3.0% and Mo-SBA-15-5.1% illustrate a slightly higher 1-butene conversion. However, the Mo-SBA-15-10.8% exhibited decreased 1-butene conversion and propene selectivity. The TEM study in Fig. 1f confirmed that the well-ordered mesoporous structure collapsed in Mo-SBA-15-10.8% due to the incorporation of too many Mo species, resulting in a poor catalytic performance even at a high Mo loading. The effect of reaction temperature on the catalytic performance is shown in Fig. 11. The initial 1-butene conversion and propene selectivity increase with an increase in the reaction temperature. However, the 1-butene conversion and propene selectivity at 500 °C decreased at longer reaction times, possibly due to the formation of olefin with a high molecular weight at high temperatures.

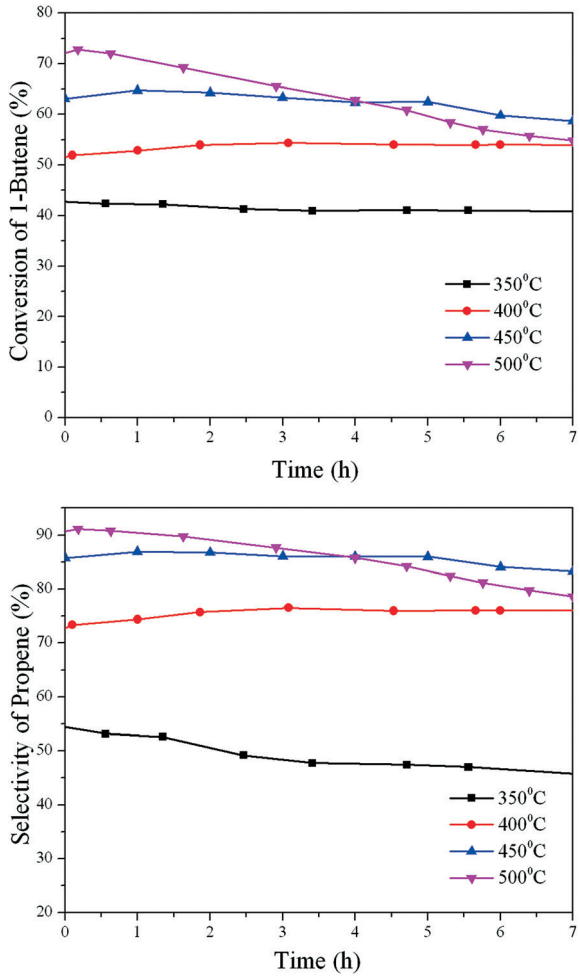

Fig. 11 1-Butene conversion (upper panel) and propene selectivity (lower panel) over Mo-SBA-15-3.0% catalysts at different reaction temperatures. Reaction conditions: P = 0.1 MPa; 1-C_4H_8/C_2H_4 = 1/2; WHSV (1-C_4H_8 + C_2H) of 2.0 h^{-1}; Mo-containing catalyst = 1.0 g.

To investigate the carbon deposition, thermogravimetric analysis under an air atmosphere was performed for the spent catalysts after a reaction time of 7 h. Fig. 12 shows the TGA and DTA curves of the spent Mo-SBA-15-3.0%, MoO_3/SBA-15-3.0%, and MoO_3/SiO_2-3.0% catalysts. Carbon deposition decreased with the following sequence: MoO_3/SiO_2-3.0% > Mo-SBA-15-3.0% > MoO_3/SBA-15-3.0%. Peaks around 410 °C were observed in DTA curves for supported MoO_3/SiO_2, whereas no obvious peaks were found for doped Mo-SBA-15 and MoO_3/SBA-15, suggesting that the distribution of high molecular weight compounds over the supported Mo-SBA-15 is significantly different from that over the mesoporous Mo-containing catalysts.

Among doped Mo-SBA-15, supported MoO_3/SBA-15 and MoO_3/SiO_2 catalysts, Mo-SBA-15 showed the best catalytic performance for the metathesis of 1-butene and ethene to propene. Doped Mo-SBA-15 exhibited a well-ordered mesoporous structure, the highest surface area, and a high concentration of Mo^{5+} species, which is beneficial to the catalytic performance. The supported MoO_3/SBA-15 catalysts also

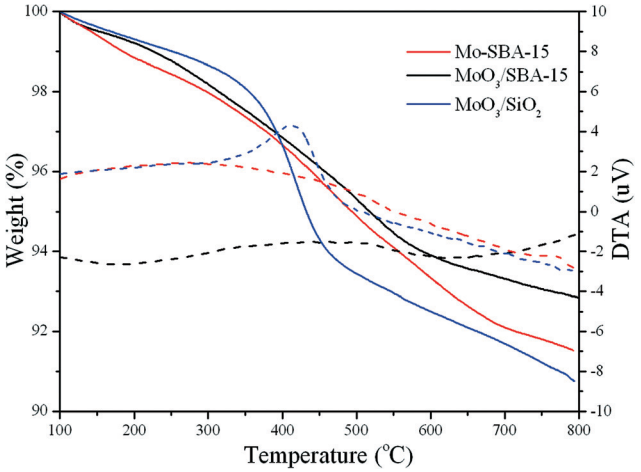

Fig. 12 TGA (—) and DTA (---) curves of different catalysts after a reaction time of 7 h for Mo-SBA-15-3.0% (red), MO_3/SBA-15-3.0% (black), and MO_3/SiO_2-3.0% (blue).

contained a well-ordered mesoporous structure, but some of the pores were blocked by the impregnation method with the absence of Mo^{5+} species, thus resulting in a relatively good catalytic performance. In contrast, traditional supported MoO_3/SiO_2 catalysts showed the lowest MoO_3 dispersion, the lowest surface area, and the absence of Mo^{5+} species, resulting in the worst catalytic performance. It is concluded that the doping method can maintain the well-ordered mesoporous structure of SBA-15 and effectively disperse Mo species with a high concentration of Mo^{5+} species. The superior catalytic performance of the Mo-SBA-15 catalysts is ascribed to their superior physicochemical properties by the doping method.

4 Conclusions

This study first compared the catalytic performance of the doped mesoporous Mo-SBA-15, supported mesoporous MoO_3/SBA-15 and supported traditional MoO_3/SiO_2 catalysts for the metathesis reaction of 1-butene and ethene to propene. Various techniques, such as XRD, TEM, Raman, BET, UV-DRS, IR and XPS, were used to characterize the obtained materials. The characterization results illustrated that the Mo species were incorporated into the SBA-15 framework with a high concentration of Mo^{5+} species for Mo-SBA-15 whereas MoO_3 nanoparticles were encapsulated within the channels of SBA-15 for MoO_3/SBA-15, and localized on the surface of the SiO_2 support for MoO_3/SiO_2. The catalytic performance of doped Mo-SBA-15 was better than that of the supported MoO_3/SBA-15 and MoO_3/SiO_2 catalysts. The 1-butene conversion and propene selectivity over the 3.0 wt% Mo-SBA-15 catalyst were around 62.4 and 85.6% at the reaction conditions of 450 °C and 0.1 MPa, respectively. In contrast, 1-butene conversion/propene selectivity over 3.0 wt% supported MoO_3/SBA-15 and MoO_3/SiO_2 were 55.8/77.2 and 50.0%/74.0% at the same reaction conditions, respectively. The superior catalytic performance of the Mo-SBA-15 catalysts

for the metathesis of 1-butene and ethene to propene was assigned to their superior physicochemical properties from the doping method. This work demonstrated a good example of enhanced catalytic performances by the doping method and could be extended to other heterogeneous catalytic reactions.

Acknowledgements

S.Z. thanks the Ministry of Science and Technology of China (grant no. 2012DFA40550) for financial supports. D.H. thanks National Science Foundation (grant no. 11375091), Ningbo Municipal Natural Science Foundation (grant no. 2011A610171) and Zhejiang Provincial Top Key Discipline of Physics (grant no. xkzw103). H.Y. thanks the financial support from Ningbo Municipal Natural Science Foundation (grant no. 2013A610038).

References

1 S. J. Connon, M. Rivard, M. Zaja and S. Blechert, *Adv. Synth. Catal.*, 2003, **345**, 572–575.
2 S. Connon and S. Blechert, Recent Advances in Alkene Metathesis, in *Ruthenium Catalysts and Fine Chemistry*, Springer, Berlin, Heidelberg, 2004.
3 S. J. Connon and S. Blechert, *Angew. Chem., Int. Ed.*, 2003, **42**, 1900–1923.
4 S. Shahane, C. Bruneau and C. Fischmeister, *ChemCatChem*, 2013, **5**, 3436–3459.
5 J. C. Mol, *J. Mol. Catal. A: Chem.*, 2004, **213**, 39–45.
6 J. Yuan, E. M. Townsend, R. R. Schrock and A. S. Goldman, *Adv. Synth. Catal.*, 2011, **353**, 1985–1992.
7 X. Li, D. Zhang, X. Zhu and F. Chen, *J. Mol. Catal. A: Chem.*, 2013, **372**, 121–127.
8 P. Amigues, Y. Chauvin, D. Commereuc and C. T. Hong, *J. Mol. Catal.*, 1991, **65**, 39–50.
9 H. Balcar, R. Hamtil, N. Žilková and Z. Zhang, *Appl. Catal., A*, 2007, **320**, 56–63.
10 S. Huang, H. Liu, L. Zhang and S. Liu, *Appl. Catal., A*, 2011, **404**, 113–119.
11 D. P. Debecker, B. Schimmoeller, M. Stoyanova and C. Poleunis, *J. Catal.*, 2011, **277**, 154–163.
12 D. Zhang, X. Li, S. Liu and X. Zhu, *Appl. Catal., A*, 2014, **472**, 92–100.
13 B. Netiworaruksa, S. Phatanasri, P. Praserthdam and W. Phongsawat, *Bulg. Chem. Commun.*, 2013, **45**, 191–196.
14 D. P. Debecker, K. Bouchmella, M. Stoyanova and U. Rodemerck, *Catal. Sci. Technol.*, 2012, **2**, 1157–1164.
15 P. Topka, H. Balcar, J. Rathouský, N. Žilková, F. Verpoort and J. Čejka, *Microporous Mesoporous Mater.*, 2006, **96**, 44–54.
16 T. Ookoshi and M. Onaka, *Chem. Commun.*, 1998, 2399–2400.
17 J. Handzlik, M. Czernecki, A. Shiga and P. Sliwa, *Polymer*, 2012, **991**, 174–181.
18 S. Liu, S. Huang, W. Xin and J. Bai, *Catal. Today*, 2004, **93–95**, 471–476.
19 H. Balcar and J. Čejka, *Coord. Chem. Rev.*, 2013, **257**, 3107–3124.
20 T. I. Bhuiyan, P. Arudra, M. N. Akhtar and A. M. Aitani, *Appl. Catal., A*, 2013, **467**, 224–234.
21 H. Balcar, D. Mishra, E. Marceau and X. Carrier, *Appl. Catal., A*, 2009, **359**, 129–135.
22 Y. C. Lou, Q. H. Tang, H. R. Wang and B. T. Chia, *Appl. Catal., A*, 2008, **350**, 118–125.
23 T. Ressler, A. Walter, Z. D. Huang and W. Bensch, *J. Catal.*, 2008, **254**, 170–179.
24 J. A. Melero, J. Iglesias, J. M. Arsuaga and J. Sainz-Pardo, *Appl. Catal., A*, 2007, **331**, 84–94.
25 B. Hu, H. Liu, K. Tao and C. Xiong, *J. Phys. Chem. C*, 2013, **117**, 26385–26395.
26 D. Zhao, J. Sun, Q. Li and G. D. Stucky, *Chem. Mater.*, 2000, **12**, 275–279.
27 D. Zhao, J. Feng, Q. Huo and N. Melosh, *Science*, 1998, **279**, 548–552.
28 C. M. Yang, P. H. Liu, Y. F. Ho and C. Y. Chiu, *Chem. Mater.*, 2002, **15**, 275–280.
29 S. Doniach and M. Sunjic, *J. Phys. C: Solid State Phys.*, 1970, **3**, 285.
30 J. G. Choi and L. T. Thompson, *Appl. Surf. Sci.*, 1996, **93**, 143–149.
31 J. P. Thielemann, G. Weinberg and C. Hess, *ChemCatChem*, 2011, **3**, 1814–1821.
32 M. R. Smith, L. Zhang, S. A. Driscoll and U. S. Ozkan, *Catal. Lett.*, 1993, **19**, 1–15.
33 L. Petrakis, P. L. Meyer and T. P. Debies, *J. Phys. Chem.*, 1980, **84**, 1020–1029.
34 K. Oshikawa, M. Nagai and S. Omi, *J. Phys. Chem. B*, 2001, **105**, 9124–9131.
35 L. Hu, S. Ji, Z. Jiang and H. Song, *J. Phys. Chem. C*, 2007, **111**, 15173–15184.
36 H. Aritani, O. Fukuda, A. Miyaji and S. Hasegawa, *Appl. Surf. Sci.*, 2001, **180**, 261–269.
37 J. P. Thielemann, T. Ressler, A. Walter and G. Tzolova-Müller, *Appl. Catal., A*, 2011, **399**, 28–34.
38 A. Duan, G. Wan, Z. Zhao and C. Xu, *Catal. Today*, 2007, **119**, 13–18.
39 Y. J. Do, J. H. Kim, J. H. Park and S. S. Park, *Catal. Today*, 2005, **101**, 299–305.
40 H. Zhang, C. Tang, C. Sun and L. Qi, *Microporous Mesoporous Mater.*, 2012, **151**, 44–55.
41 Y. Shao, L. Wang, J. Zhang and M. Anpo, *J. Phys. Chem. B*, 2005, **109**, 20835–20841.